# Electrical modulation of the complex refractive index in mid-infrared quantum cascade lasers

**J. Teissier,[1] S. Laurent,[1] C. Manquest,[1] C. Sirtori,[1] A. Bousseksou,[2] J. R. Coudevylle,[2] R. Colombelli,[2] G. Beaudoin,[3] and I. Sagnes[3]**

[1]*Laboratoire Matériaux et Phénomènes Quantiques, Université Paris Diderot- CNRS. UMR 7162, 75013 Paris, France*

[2]*Institut d'Electronique Fondamentale, UMR8622 CNRS, Univ. Paris Sud, 91405 Orsay, France*

[3]*Laboratoire Photonique et Nanostructure CNRS, UPR 20, 91460 Marcoussis, France*

**jean.teissier@gmail.com*

**Abstract:** We have demonstrated an integrated three terminal device for the modulation of the complex refractive index of a distributed feedback quantum cascade laser (QCL). The device comprises an active region to produce optical gain vertically stacked with a control region made of asymmetric coupled quantum wells (ACQW). The optical mode, centered on the gain region, has a small overlap also with the control region. Owing to the three terminals an electrical bias can be applied independently on both regions: on the laser for producing optical gain and on the ACQW for tuning the energy of the intersubband transition. This allows the control of the optical losses at the laser frequency as the absorption peak associated to the intersubband transition can be electrically brought in and out the laser transition. By using this function a laser modulation depth of about 400 mW can be achieved by injecting less than 1 mW in the control region. This is four orders of magnitude less than the electrical power needed using direct current modulation and set the basis for the realisation of electrical to optical transducers.



**OCIS codes:** (140.0140) Lasers and laser optics; (250.0250) Optoelectronics.

## References and links

1. Y. Bai, S. Slivken, S. R. Darvish, and M. Razeghi, "Room temperature continuous wave operation of quantum cascade lasers with 12.5% wall plug efficiency," Appl. Phys. Lett. **93**(2), 021103 (2008).
2. R. F. Curl, F. Capasso, C. Gmachl, A. A. Kosterev, B. McManus, R. Lewicki, M. Pusharsky, G. Wysocki, and F. K. Tittel, "Quantum cascade lasers in chemical physics," Chem. Phys. Lett. **487**(1-3), 1–18 (2010).
3. F. Capasso, C. Sirtori, and A. Y. Cho, "Coupled quantum well semiconductors with giant electric field tunable nonlinear optical properties in the infrared," IEEE J. Quantum Electron. **30**(5), 1313–1326 (1994).
4. J. Teissier, S. Laurent, C. Sirtori, H. Debrégeas-Sillard, F. Lelarge, F. Brillouet, and R. Colombelli, "Integrated quantum cascade laser-modulator using vertically coupled cavities," Appl. Phys. Lett. **94**(21), 211105 (2009).
5. R. Paiella, F. Capasso, C. Gmachl, H. Y. Hwang, D. L. Sivco, A. L. Hutchinson, A. Y. Cho, and H. C. Liu, "Monolithic active mode locking of quantum cascade lasers," Appl. Phys. Lett. **77**(2), 169 (2000).
6. C. Y. Wang, L. Kuznetsova, V. M. Gkortsas, L. Diehl, F. X. Kärtner, M. A. Belkin, A. Belyanin, X. Li, D. Ham, H. Schneider, P. Grant, C. Y. Song, S. Haffouz, Z. R. Wasilewski, H. C. Liu, and F. Capasso, "Mode-locked pulses from mid-infrared Quantum Cascade Lasers," Opt. Express **17**(15), 12929–12943 (2009).
7. G. Chen, C. G. Bethea, R. Martini, P. D. Grant, R. Dudek, and H. C. Liu, "High-speed all-optical modulation of a standard quantum cascade laser by front facet illumination," Appl. Phys. Lett. **95**(10), 101104 (2009).
8. A. Lyakh, R. Maulini, A. Tsekoun, R. Go, and C. K. N. Patel, "Intersubband absorption of quantum cascade laser structures and its application to laser modulation," Appl. Phys. Lett. **92**(21), 211108 (2008).
9. E. Benveniste, S. Laurent, A. Vasanelli, C. Manquest, C. Sirtori, F. Teulon, M. Carras, and X. Marcadet, "Measurement of gain and losses of a midinfrared quantum cascade laser by wavelength chirping spectroscopy," Appl. Phys. Lett. **94**(8), 081110 (2009).
10. P. Holmström, P. Jänes, U. Ekenberg, and L. Thylén, "Efficient infrared electroabsorption with 1 V applied voltage swing using intersubband transitions," Appl. Phys. Lett. **93**(19), 191101 (2008).
11. Band structure: The layer sequence of one period in nanometer, is 3.1/**1.7**/3.1/**1.6**/2.8/***1.8***/*2.4*/***2.4*** /*2.4*/**2.4**/2.6/**4.1**/1.7/**1.0**/5.3/**1.2**/5.2/**1.2**/4.4/**2.1** where $In_{0.52}Al_{0.48}As$ layers are in bold and the underlined numbers correspond to the doped layers ($10^{17}$ $cm^{-3}$).

#149761 - $15.00 USD Received 23 Jun 2011; revised 30 Aug 2011; accepted 26 Sep 2011; published 5 Jan 2012

12. M. Helm, *Intersubband Transitions in Quantum Wells: Physics and Device Applications I,* edited by H. C. Liu and F. Capasso, (Academic, 2000), vol. 62, pp. 1–99.
13. K. L. Campman, H. Schmidt, A. Imamoglu, and A. C. Gossard, "Interface roughness and alloy-disorder scattering contributions to intersubband transition linewidths," Appl. Phys. Lett. **69**(17), 2554 (1996).
14. From top to buffer: GaInAs ($5.10^{18}$cm$^{-3}$, 300nm), InP ($1.10^{17}$cm$^{-3}$, 2.1μm), GaInAs($5.10^{16}$cm$^{-3}$, 0.4μm), active region, GaInAs($5.10^{16}$cm$^{-3}$, 0.4μm), InP($1.10^{17}$cm$^{-3}$, 2μm), GaInAs ($1.10^{17}$ cm$^{-3}$, 500nm), 5 periods of coupled QW separated by 300Å of AlInAs, GaInAs ($5.10^{16}$ cm$^{-3}$, 1μm), InP ($2.10^{17}$ cm$^{-3}$, 2μm), buffer InP ($10^{17}$ cm$^{-3}$).
15. E. Benveniste, A. Vasanelli, A. Delteil, J. Devenson, R. Teissier, A. Baranov, A. M. Andrews, G. Strasser, I. Sagnes, and C. Sirtori, "Influence of the material parameters on quantum cascade devices," Appl. Phys. Lett. **93**(13), 131108 (2008).
16. H. C. Liu, J. Li, M. Buchanan, and Z. R. Wasilewski, "High-frequency quantum-well infrared photodetectors measured by microwave-rectification technique," IEEE J. Quantum Electron. **32**(6), 1024–1028 (1996).

## 1. Introduction

Progresses in the development of quantum cascade lasers (QCL) have led recently to the demonstration of continuous wave operation at room temperature with Watt-level output powers [1]. This performance demonstrates that mid infrared QCLs are ideal devices for spectroscopic applications, in particular trace gas detection techniques [2], and show their potential also for free space optical data communication. Both these applications could benefit from the development of compact mid infrared emitting devices in which new functionalities are inserted, primarily the electrical control of the complex refractive index for amplitude and frequency modulation purposes. Moreover, it is of great interest to obtain this function without direct modulation of the injected power, which implies, even for the best devices to modulate 5 – 10 Watt of electrical power. This could be readily obtained using three terminal devices in which a control function is addressed independently from the laser driving current.

In this paper, we demonstrate that it is possible to modulate the frequency and amplitude of a quantum cascade laser by inserting into the device a control section in the transverse direction operated by a third terminal. This function has been enabled by exploiting the linear Stark effect of the intersubband (ISB) transitions in asymmetric coupled quantum wells (ACQW), and their related absorption [3]. In this configuration the peak absorption wavelength can be tuned as a function of the applied voltage on the control section. In a previous report [4], we have given a proof of principle that such a system can electrically modulate the laser cavity losses; our device permitted to modulate 12 mW of optical power by injecting 1 mW of electrical power. In this work, we demonstrate a modulation depth of more than 400 mW for less than 1 mW of injected electrical power. This has been obtained in lasers showing better performances by increasing the doping of the control area and its overlap with the optical mode. Moreover, the ability to modulate high absorption coefficients and the implementation of a DFB cavity, has led us to the demonstration of the electrical modulation of the real part of the refractive index and the consequent tuning of the laser emission wavelength. Finally, we have also studied the frequency response of these devices up to 1 GHz.

## 2. Description of the three terminal devices

Intensity modulation of a quantum cascade laser has been achieved up to now either by a direct modulation of the driving current [5,6] or by an all optical modulation technique [7]. The first method yielded to date cut-off frequencies in the order of 10 GHz, limited by the RC-constant of the circuits and not from the intrinsic response of the laser. The typical operating condition for state of the art QCLs is 10 – 15 V for few hundreds of mA of injected current. This implies that to obtain a significant modulation depth of the optical output an electrical power in the order of a few watt (20 to 30 dBm) has to be injected. This causes a linewidth enhancement due to thermal chirp. On the other hand, all optical modulation, which can take advantage of the extremely high bandwidth of femtosecond near-infrared lasers, necessitates focussing the modulating beam on the QC laser front facet with a consequent increase in the complexity of the system.

Ref [8] suggests an alternative approach to modulate the optical losses: A QC laser is divided in two sections. In this configuration the second section is used below its transparency

#149761 - $15.00 USD Received 23 Jun 2011; revised 30 Aug 2011; accepted 26 Sep 2011; published 5 Jan 2012

point [9] so to modulate the losses using the residual ISB absorption. With this method, one can potentially obtain a monolithically integrated intracavity modulation of QCLs with suppressed thermal chirp. This could be an advantage for photoacoustic spectroscopy and in general for all spectroscopy, for which a modulated excitation beam with no linewidth enhancement is required.

Our approach presents the same advantage as it uses a very low voltage swing [10] to modulate the cavity losses. Moreover, thanks to the inclusion of a third terminal it allows the electrical injection in the laser active region independently from the amplitude of the optical losses activated in the control region. Figure 1 shows a schematic of the three terminal device studied and developed in this paper. Two core sections, the active region and the ACQW control region, have been stacked vertically. They are separated by an n doped InP cladding layer that serves as a ground contact. On the top of the laser ridge, a first order Bragg grating has been etched in order to obtain a distributed feedback operation, thus monomode emission.

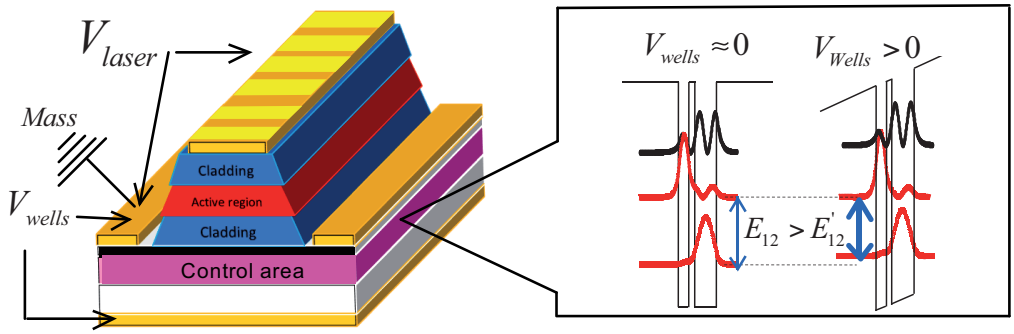


Fig. 1. Left: Schematic view of a three terminals device with a DFB on top. Right: conduction band (BC) profile of the AQW with the associated energy subbands and moduli squared of the wavefunctions: The wells are respectively 60 Å and 22 Å thick and separated by a 16 Å barrier.

The active region, whose details can be found in Ref [11], consists of 36 periods of a four quantum well double phonon resonance design grown on InP. Figure 1, right panel, represents the coupled quantum well structure and the associated energy levels and wave functions of the control region. Figure 2 shows that the ISB separation energy $E_{12}$ between the first two levels of the structure is a linear function of the electric field applied to the wells. This has been extensively studied in Ref [3]. where it was shown that the Stark shift can be very well approximated by the potential drop between the centres of the two wells. Figure 2 shows both the calculated and measured intersubband transition energies. The discrepancy observed between the data and the simulation will be discussed in section 4. By tuning the absorption wavelength over the spectral range of the laser emission, we can add controllable optical losses and modulate the laser complex effective refractive index. Such a device can thus electrically modulate simultaneously both the intensity *and* the frequency of the laser.

#149761 - $15.00 USD Received 23 Jun 2011; revised 30 Aug 2011; accepted 26 Sep 2011; published 5 Jan 2012

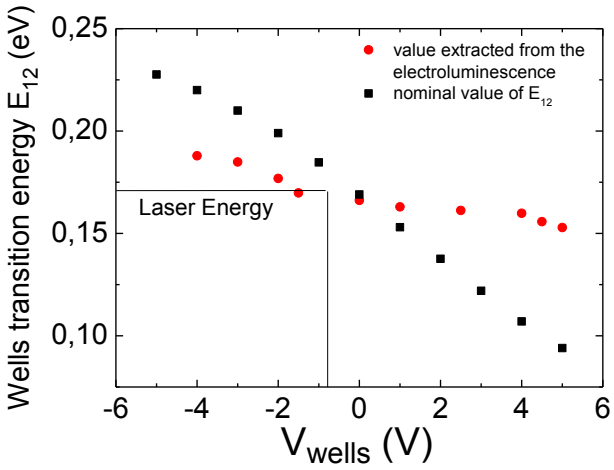


Fig. 2. Squares: Calculated intersubband transition energy $E_{12}$ between the two first levels of AQW calculated as a function of bias applied on the wells. Dots: values extracted from the electroluminescence measurements.

The design of the laser cavity has to comply with two criteria: an efficient lateral extraction of the current pumping the active region and an optimized absorption coefficient induced by the ACQW. The highest modulation depth can be obtained by limiting the thickness of the InP doped layer separating the active from the control regions, thus inducing a high modal overlap with the ACQW. However, this could be detrimental to a good lateral current injection as it would increase the access resistance. For our design we have chosen to connect the two regions using a 2-µm-thick InP layer *n*-doped to $10^{17}$ cm$^{-3}$. An estimation of the lateral resistance of this contact yields to ~1 Ω. To quantify the additional losses introduced by the ACQWs, we calculate the absorption coefficient following Ref [12]:

$$\alpha_{wells}(E) = \frac{n_S e^2 \mathrm{h}}{2\sqrt{\ln 2}\varepsilon_0 c n_{eff} m^*} \frac{f_{12}}{\gamma} \exp\left(-\frac{(E_{12}-E)^2}{\gamma^2}\right) \frac{\Gamma_{wells}}{L_{wells}} \qquad (1)$$

In this expression, we assume that $\alpha_{wells}$ has a Gaussian line shape typical of a spatially diagonal transition [13]. The constants $e$, $\hbar$, $\varepsilon_0$ and $c$ are respectively the electron charge, Planck's constant divided by 2π, the vacuum dielectric constant and the speed of light. $n_{eff}$ is the effective refractive index, E the energy, $m^*$ the electron effective mass, $f_{12}$ and $\sqrt{\ln 2}\,\gamma$ the oscillator strength and the half width at half maximum of the transition (HWHM). $L_{wells}$ is the length of one period of the coupled quantum wells heterostructure, $n_S$ is the sheet density and $\Gamma_{wells}$ is the mode overlap factor with the control region.

The structure is optimised by first calculating the two dimensional optical mode and choosing the value of the overlap $\Gamma_{wells}$. The exact design of the structure is given in ref [14]. The model confirms that the cladding layer inserted between the control and active regions can be as thick as 2 µm, while still maintaining a sufficient overlap of the laser mode with the control region. ($\Gamma_{wells}$ ~1% according to our simulations). In order to obtain strong modulation depth, the value of the additional losses $\alpha_{wells}$ has to be set a few times the value of the waveguide losses of our device. For quantum cascade lasers in the 7 µm wavelength range, typical values of the total losses are 5-10 cm$^{-1}$. This implies that the losses introduced by the control section have to amount to approximately 30-40 cm$^{-1}$. With $\Gamma_{wells}$ ~1%, as discussed above, the value of $\alpha_{wells}$ can be adjusted by choosing the doping concentration of the ACQW. By introducing in Eq. (1) the nominal values of $L_{wells}$ = 399 Å, $f_{12}$ = 0.4 and $n_S = 10^{12}$ cm$^{-2}$, we obtain a peak absorption coefficient, $\alpha_{wells}$ = 36 cm$^{-1}$, in agreement with the desired value.

#149761 - $15.00 USD Received 23 Jun 2011; revised 30 Aug 2011; accepted 26 Sep 2011; published 5 Jan 2012

Figure 3 shows a 1D numerical simulation of the optical mode together with the refractive index profile of the structure. In the inset a close-up of the control area is illustrated. The overlap factor between the optical mode and the control region has been designed to obtain the controllable intersubband losses four times higher than typical waveguide losses.

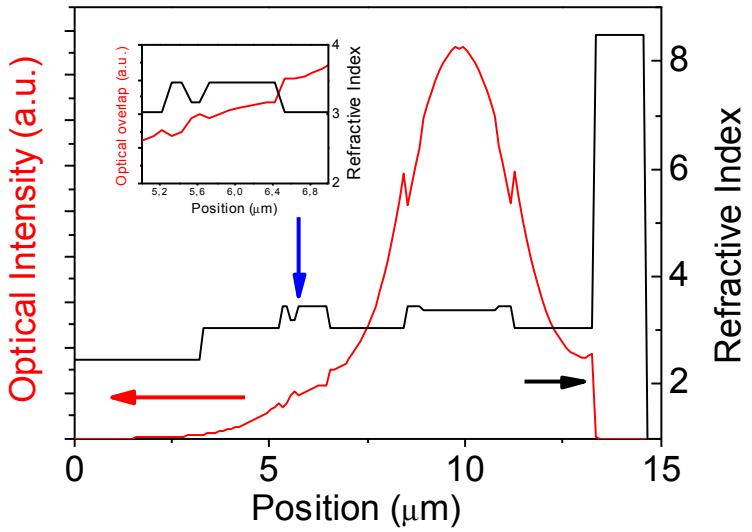


Fig. 3. 1D simulation of the optical mode inside the acvity. In red is the optical intensity and in black the refractive index curve. The insert is a zoom on the control area overlap.

The structure was grown by metal-organic chemical vapor deposition. Following the fabrication of the distributed Bragg mirror by electronic beam lithography and wet chemical etching, ridge lasers were fabricated by etching the semiconductor down to the bottom of the active region. After protecting again the ridge, we can further etch again the control region in order to limit the parasitic capacitance. An insulating layer is then deposited and opened on the surface of the ridge and at the bottom of it to define the top metal contacts. The two top contacts are fabricated using a lift-off technique in one side of the ridges, the backside of the structure is used as third contact. Each laser was soldered junction up on a copper mount.

Figure 4 shows the light-current-voltage curves at 77K for a 2-mm long and 24-μm wide device for two different applied voltages to the ACQWs, $V_{wells}$. The experiments are performed at 77 K and not at 300 K due to the important absorption of the control region. As the resistivity of the control area increases as a function of temperature, we decided to operate at 77K as the gain of the laser section would not be able to compensate the maximal losses of the control area at room temperature. This would result in incomplete curves due to the lack of sufficiently elevated optical gain. The laser operated in pulsed mode with a duty cycle of 0.05%. For $V_{wells} = -5$V, the ISB transition in the control section does not absorb and the measured threshold current density ($J_{th}$) is the same (~1 kA/cm$^2$) as the one obtained for an identical, reference device without the control region. This proves that the insertion of the control region doesn't substantially change the laser mode profile leaving the threshold density of the laser unaffected. However the differential resistance of the device is higher in the structure with the control section due to the lateral current injection, 4.5 Ω instead of 1.4 Ω for the reference sample. This relatively high resistance value could be reduced by optimising our contact fabrication procedure. In fact we have measured a contribution to the lateral resistance originating from the contact in the order of 1 Ω. A higher doping level in the intermediate layers could reduce this value but it would increase the optical losses of the cavity.

#149761 - $15.00 USD Received 23 Jun 2011; revised 30 Aug 2011; accepted 26 Sep 2011; published 5 Jan 2012

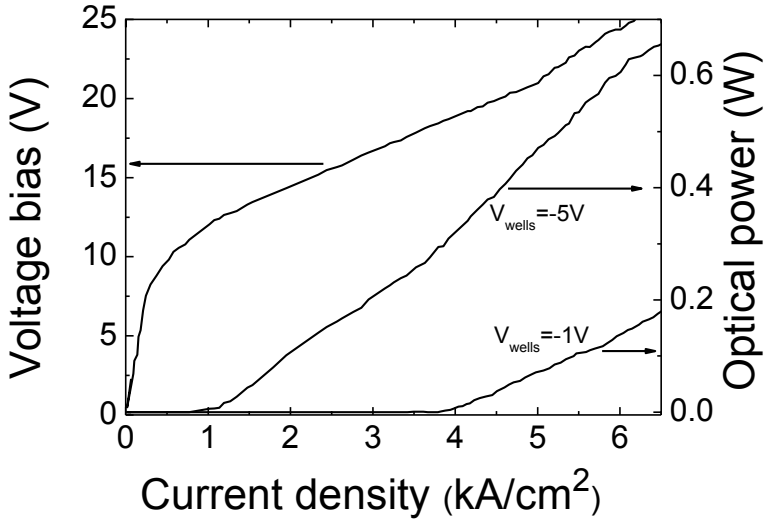


Fig. 4. Light current voltage characteristics for two bias applied on the wells region. The V(I) curves are the same for the two different applied voltages $V_{wells}$.

### 3. Amplitude modulation of the laser

An evident decrease of the cavity optical losses appears when we apply a negative bias to the control region as it is illustrated in Fig. 4 where by changing $V_{wells}$ from −1V to −5V, the threshold current density decreases by almost a factor of 4. To evaluate the efficiency of the control region in modulating the light intensity, we measured (Fig. 5) the dependence of the laser peak power $P$ and of the threshold current as a function of the bias ($V_{well}$) applied to the ACQWs, while keeping a constant injected current in the active region. The results, for an injected current density of 6.3 kA/cm$^2$ are presented in Fig. 5(b). We first notice that the dependence of both the laser power $P$ and the threshold current $J_{th}$ as a function of the ACQW bias reproduces the characteristic line shape of an ISB transition. This is expected as the transition energy of the ACQW evolves linearly with the bias applied on the control region. The peak of the losses is reached when the ISB transition is at the same energy as the laser. This occurs for $V_{wells}$ = −1V, in fair agreement with our simulations which predict a value of 0V.

From Fig. 5a, we can observe that the absorption of the wells increases $J_{th}$ up to 3.6 times, which gives a maximum relative change of the absorption coefficient: $\frac{\Delta\alpha_{tot}}{\alpha_{tot}} = \frac{\alpha_{wells}(E_{laser})}{\alpha_{tot}} = \frac{\Delta J_{th}}{J_{th}} = 2.4$, with $\alpha_{tot}$ the total losses. By applying the technique developed in [9], we have measured the loss coefficient $\alpha \approx 9.3 cm^{-1}$ (where $\alpha = \frac{4\pi \,\mathrm{Im}(n)}{\lambda}$ is the propagation losses), when there are no extra losses introduced by the control region. From this value, we estimate that the maximum loss added to the cavity is $\alpha_{wells}(E_{laser}) = 2.4\alpha = 22.3\ cm^{-1}$, which gives $\Gamma_{wells}$~*0.6%*, in good agreement with our design. In Fig. 5b, we plot the optical modulation contrast, $\Delta P / P_{max}$ as a function of the bias on the control region, $V_{wells}$. This $\Delta P$ is defined as $P_{max}$ - $P(V_{wells})$, where $P(V_{wells})$ is the emitted power for different bias voltage on the ACQW region and $P_{max}$ is the highest measured power. $\Delta P$~450 mW at J = 6.3 kA/cm$^2$. For higher current densities even though the modulation contrast decreases, $\Delta P$ keeps on increasing since the slope efficiency of the laser at $V_{wells}$ = −5V (absorption OFF) is higher than the one at $V_{wells}$ = −1 V(absorption ON), due to the

#149761 - $15.00 USD Received 23 Jun 2011; revised 30 Aug 2011; accepted 26 Sep 2011; published 5 Jan 2012

higher cavity losses. These two different slopes explain the increase of the HWHM in Fig. 5, going from (a) to (b).

The most striking result is that such a modulation depth is obtained by injecting an electrical power of less than 1 mW into the control region, as it is illustrated in Fig. 5a. We have therefore realised a function (a power switch) that allows the control of the laser emission with very small electrical power dissipation, if compared to a direct current modulation. This could, e.g., avoid the linewidth enhancement due to thermal shifts typically observed for low frequency direct modulation of the driving current, which is due to thermal effects [8,10].

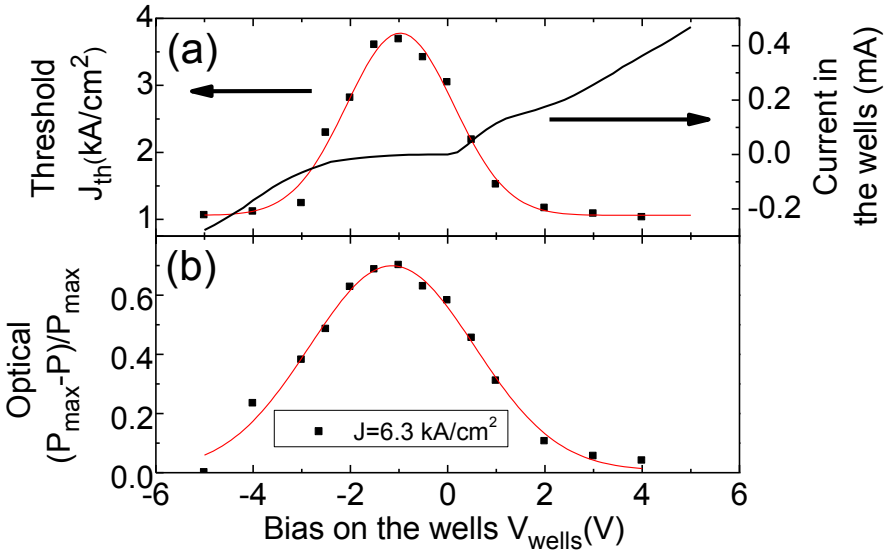


Fig. 5. (a) Laser threshold current density (squares, left) and current passing through the wells (right) as a function of the CW bias applied to the wells. (b) Optical modulation depth, $\Delta P$ as a function of the CW bias applied to the wells.

## 4. Frequency modulation of the laser

To characterize the influence of the control region on the frequency of the laser, we measured the electroluminescence at J = 0.66*$J_{th}$ (for $V_{wells}$ = −5 V) for different continuous wave bias applied on the ACQW region. The results are given in Fig. 6. When the ACQWs don't absorb, the spectral emission is the sum of two peaks representing the laser transition and the transition between the injector level and the lower level of the laser transition [15]. When $V_{wells}$ increases, the wells transition energy is shifted toward low energies and we can observe the progressive overlap of the ACQWs absorption spectrum with the electroluminescence spectrum. The curves at $V_{wells}$ = −7 V and + 6 V are practically identical since the ACQWs absorption spectrum is respectively at higher and lower energy than the electroluminescence spectrum.

#149761 - $15.00 USD Received 23 Jun 2011; revised 30 Aug 2011; accepted 26 Sep 2011; published 5 Jan 2012

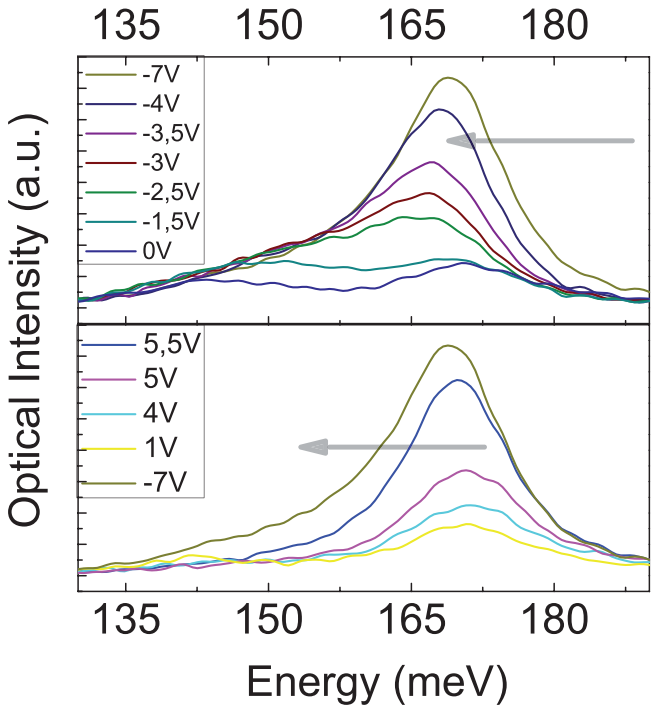


Fig. 6. Electroluminescence of the device (J = 66% of Jth min) for several voltages applied on the wells.

From the electroluminescence measurements, which we define as $Lum_V(E)$, we can extract the ACQWs transition energy as a function of $V_{wells}$. The electroluminescence has two components. One originates from the guided mode, and it is subject to the control area absorption. The other one is the isotropic emission. We define $Lum_{ref}(E)e^{-L\alpha_{wells}(E)}$ the guided mode component, where $Lum_{ref}(E)$ is the emission of the guided mode without absorption, L is the length of the cavity. The isotropic part is proportional to $Lum_{ref}(E)$. We thus obtain $Lum_V(E) = Lum_{ref}(E)(Ae^{-L\alpha_{wells}(E)} + B)$. By fitting $Lum_V(E)/Lum_{ref}(E)$ with $e^{-L\alpha_{wells}(E)} + B$, B being a constant, we can extract the energy position of the optical transition in the ACQW at each bias. The transition energies obtained with this procedure are reported in Fig. 2 and they are compared to the nominal, theoretically calculated values. It appears that the tuning of the transition energy with the applied electric field is smaller than expected. We attribute the difference to the fact that the exact value of the potential drop within the structure may be smaller than the external applied voltage. This could be caused by an inhomogeneous field distribution induced by the fact that the voltage is applied on a contact ~50 µm away from the laser ridge.

#149761 - $15.00 USD Received 23 Jun 2011; revised 30 Aug 2011; accepted 26 Sep 2011; published 5 Jan 2012

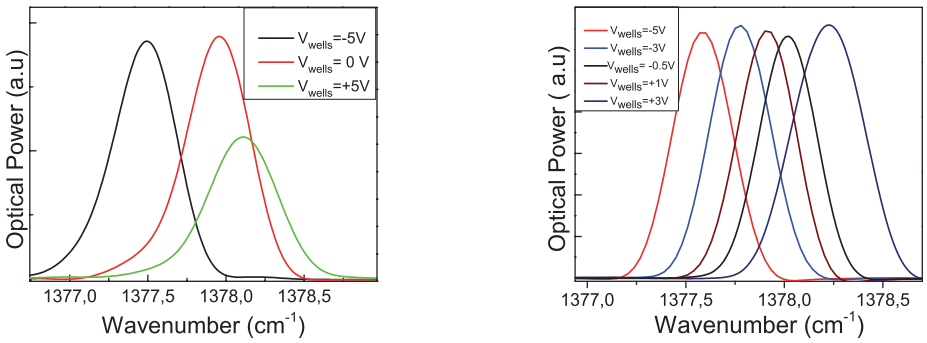


Fig. 7. (a) Spectrum of the DFB laser for three bias applied on the wells at constant laser driving. (b) Several spectrum at constant optical power. Added losses are compensated by increasing the driving current. The spectral resolution of the fast Fourrier infrared spectrometer is 0.25cm$^{-1}$.

The influence of the $V_{wells}$ bias on the laser spectrum is represented in Fig. 7. We observe a small shift of the emission wavenumber of ~0.5 cm$^{-1}$ for constant injection power in the laser part, Fig. 7(a). On Fig. 7(b) by changing the injected power on the laser part we are able to maintain a constant optical power with almost 1 cm$^{-1}$ of frequency modulation. Since the control region modulates the imaginary part of the effective index, it also modulates its real part as they are connected through Kramers Kronig relations. The DFB wavelength is given by $\lambda_{DFB} = 2n_{eff}\Lambda$, thus the control region introduces a relative wavelength change equal to.

$$\frac{\Delta\lambda_{DFB}}{\lambda_{DFB}} = \frac{\Delta n_{eff}}{n_{eff}}$$

In order to verify that the observed shift is due to the control region, we first estimated the relative change of the real part of the effective index. To do so, we determine the absorption spectrum of the control region "$\alpha_{wells}$" as a function of energy (E) for each $V_{wells}$ bias and then apply the Kramers Kronig relation of these coefficients at the energy of the laser to extract $\Delta n_{eff}(E_{laser}, V_{wells})$.

Following Eq. (1), $\alpha_{wells}$ can be written as:

$$\alpha_{wells} = A(V_{wells})\exp\left(-\frac{\left(E_{12}(V_{wells})-E\right)^2}{\gamma^2}\right)$$
$$A(V_{wells}) = \frac{n_S e^2 \mathrm{h}}{2\sqrt{\ln 2}\varepsilon_0 c n_{eff} m^*}\frac{f_{12}(V_{wells})}{\gamma}\frac{\Gamma_{wells}}{L_{wells}} \qquad (2)$$

In this expression, we assume that the HWHM of the wells transition does not evolve with the bias and we neglect the dependence of the refractive index in the denominator of $A$ since it is negligible in comparison with the evolution of $f_{12}(V_{wells})$. To determine $\alpha_{wells}$, we therefore need to know $A(V_{wells})$, $E_{12}(V_{wells})$ and $\gamma$. $E_{12}(V_{wells})$ has been deduced from the electroluminescence spectra (see section II). The maximum value of losses added to the cavity is $\alpha_{wells}(E = E_{12}, V_{wells} = -1V) = A(V_{wells} = -1\,V) = 22.7\,cm^{-1}$.

The coefficient $A(V_{wells})$ is a function of the applied bias as the oscillator strength of the diagonal transition in the ACQWs changes substantially for different applied bias. We then use our band structure calculations to estimate the oscillator strength for each bias and infer the other coefficient $A(V_{wells})$. Finally the HWHM can be found by fitting the losses deduced from Fig. 5a. The result of the fit is superimposed with the data on Fig. 8 and yields a value of $\gamma \approx 7\,meV$.

#149761 - $15.00 USD Received 23 Jun 2011; revised 30 Aug 2011; accepted 26 Sep 2011; published 5 Jan 2012

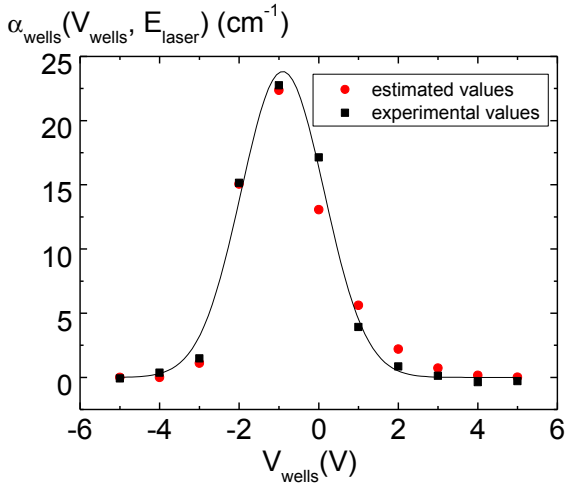


Fig. 8. Estimated and experimental values of the absorption coefficient of the wells as a function of the bias applied on the wells. The black curve is the Gaussian fit of the experimental values.

By applying Kramers-Krönig relations, we obtain the effective refractive index change and therefore the wavelength change induced by the control region. We plot on Fig. 9 the evolution - as a function of $V_{wells}$ - of both the measured and simulated effective refractive index. The agreement between the two curves is very good and leads us to the conclusion that the refractive index changes are indeed induced by bias applied to the control region. Some discrepancy between the two curves arises however at high bias. We attribute this discrepancy to a sample heating caused by the electrical power dissipated into the device, as a temperature increase can also lead to an increase of the refractive index. However, the good correlation between the two curves corroborates our hypothesis that thermal effects are playing a role at high bias. On the right axis of Fig. 9 we have plotted the injected electrical power that increases rapidly for $V_{wells} < -4$ and $V_{wells} > 3$. In these regions indeed the differences between the two curves are most pronounced.

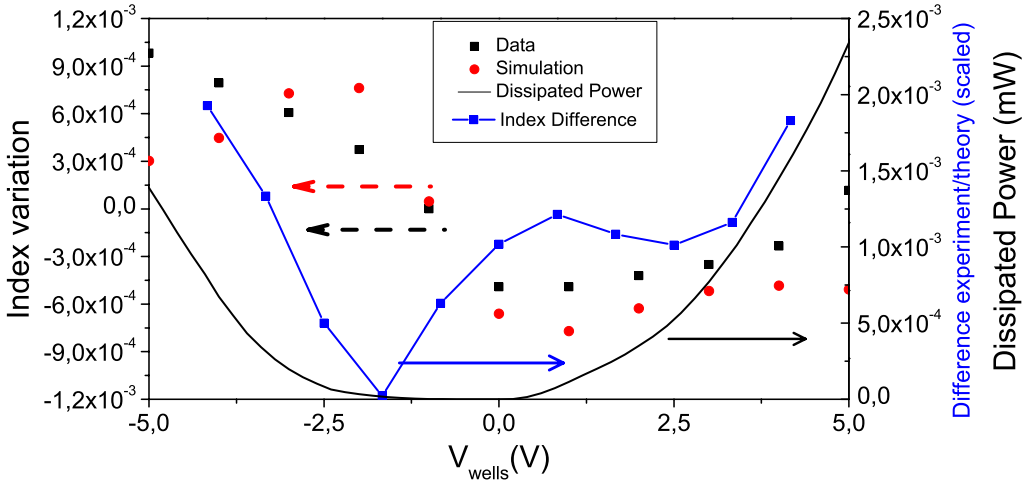


Fig. 9. Left axis: Experimental and estimated effective refractive index variation as a function of the bias applied on the wells. Right axis: black curve: electrical power injected into the wells. Blue curve: difference between the calculated index and the one observed experimentally.

#149761 - $15.00 USD Received 23 Jun 2011; revised 30 Aug 2011; accepted 26 Sep 2011; published 5 Jan 2012

## 5. Frequency cut off of the device

The modulation speed of our devices is limited by the *RC* parallel circuit that we use to inject the microwave power into the device, where $R_{wells}$ is the differential resistance and $C_{wells}$ the capacitance of the control region [16]. As shown in the inset of Fig. 10 the two contacts allow a complete separation of the cut-off frequencies, one from the QC laser and one from the control area. By using the approach developed in [16], $C_{wells}$ can be estimated by a parallel plate approximation, and the resulting $R_L C_{wells}$ ($R_L$ = 50 Ω is the load resistance) characteristic frequency of the circuit is close to 10 MHz, since the surface contact of the control region was not optimised (~500 µm*2 mm). To decrease the capacitance, we etched the control region to obtain a surface contact of ~2 mm*33 µm, thus increasing the characteristic cut off frequency to 0.12 GHz.

We measured the modulation depth of the system as a function of the frequency by using a detector with a response time smaller than 2 ns and an oscilloscope with a 3 GHz frequency cut off. The microwave signal was added to the DC ($V_{wells}$ = 0.1V) signal through a bias tee. The current density of the laser was 5.2 kA/cm$^2$. The measurements – reported in Fig. 10 - were made for two injected microwave powers of 0 dBm and 10 dBm. Our detector response time limits the measurement to frequencies smaller than 400 MHz. We can deduce from the measurement a −3 dB frequency close to 100 MHz, in good agreement with the model. We also notice that by increasing the injected power to 10 dBm we can modulate beyond the cut off frequency while still maintaining a maximum modulation depth. Since this system needs a very small electrical power to modulate, it can be used both to modulate the QCL amplitude at low frequency without any linewidth enhancement and at a frequency higher than the 3dB cut off frequency by just increasing the injected power.

In this device architecture, however, the capacitance is too high to allow a frequency response higher than 10 GHz and a further reduction of the size of the control region would be necessary to reach higher modulation frequencies. This could be realised by growing the AQWs on top of the active region and finally implementing a multi section laser.

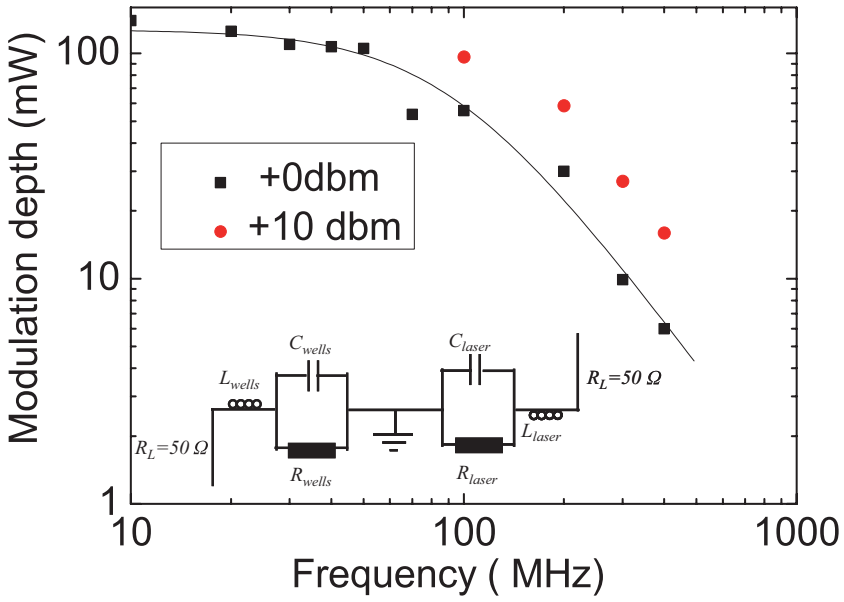


Fig. 10. Modulation depth as a function of the microwave frequency for two injected microwave powers. The black curve is a first order fit for the 0 dBm modulation depth curve. The equivalent electrical circuit of the electromodulator is shown in insert. It can be noticed that given position of the ground in the middle, the two parts are completely independent.

#149761 - $15.00 USD Received 23 Jun 2011; revised 30 Aug 2011; accepted 26 Sep 2011; published 5 Jan 2012

## 6. Conclusion

In conclusion, we have demonstrated a three-terminal-device where a control region is integrated within the cavity of a quantum cascade laser operating at $\lambda \approx 7.5$ μm. The control region allows the modulation of the cavity losses and - as a consequence - of the laser output power and emission frequency. The cavity losses are modulated via the Stark effect in asymmetric quantum wells. This effect is intrinsically very fast as it does not imply carrier transport or capacitor charging across the heterostructure and could be exploited for high frequency modulation in a suitably conceived device. Moreover, the control region can be operated with very small electrical power and therefore these devices set the basis for an electrical to optical transducer, able to inscribe a microwave signal onto a mid infrared optical carrier. This integrated function could also significantely decrease the linewidth enhancement due to thermal shift which is typically observed when the injection current is directly modulated.

## Acknowledgment

The authors would like to thanks Mr Stefano Barbieri, Pierre Gellier and Wilfried Maineult (MPQ) for their help and knowledge in high frequency modulation domain. The device fabrication has been performed at the nano-center CTU-IEF-Minerve, which is partially funded by the “Conseil Général de l'Essonne”, and at the nano-center of the LPN. We gratefully acknowledge financial support from the “Agence Nationale de la Recherche” through the program ANR-06-NANO-047 MetalGuide.

#149761 - $15.00 USD Received 23 Jun 2011; revised 30 Aug 2011; accepted 26 Sep 2011; published 5 Jan 2012